UNIVERSITÀ DEGLI STUDI DI BARI

Dipartimento Interateneo di Fisica "M. Merlin"

PhD School in Physic XXXII cycle

Activity report on the first year

Supervisor:

dott.ssa G. Pugliese

PhD student:

dott. A. Gelmi

My PhD research activity is developing in the context of the Muon Upgrade project of the Compact Muon Solenoid (CMS) experiment, for the High Luminosity phase of the Large Hadron Collider (HL-LHC) at CERN. At present, three types of gas-ionization chambers are used to make up the CMS muon system: Drift Tube chambers (DT), Cathode Strip Chambers (CSC), and Resistive Plate Chambers (RPC). In view of the increase of the LHC luminosity, to maintain excellent muon triggering and reconstruction performance, the Muon system will be consolidated and the muon coverage will be extended up to eta 2.4. My activity is focusing on the Upgrade of the RPC system.

1. CMS-RPC SYSTEM UPGRADE

The RPC system covers both Barrel and Endcap regions of CMS [1,2] contributing to the trigger, reconstruction and identification of muons. It consists of 1056 RPCs, organized in 4 stations called RB1 to RB4 in the Barrel region, and RE1 to RE4 in the Endcap region, as shown in Figure 1. At HL-LHC, the instantaneous luminosity will increase up to $5 \cdot 10^{34}$ cm^{-2} s^{-1} (factor five more then the nominal LHC luminosity) and the expected integrated luminosity, over 10 years of running, will be 3000 fb^{-1}. The expected conditions in terms of background and pile-up and the probable aging of the present detectors will make the muon identification and correct p_T assignment a challenge for the muon system. In order to ensure redundancy of the muon system [3] also under the HL-LHC conditions, two upgrades [4,5] are planned on the RPC system: the consolidation of the present system and the extension of the muon coverage at the $|\eta| < 2.4$.

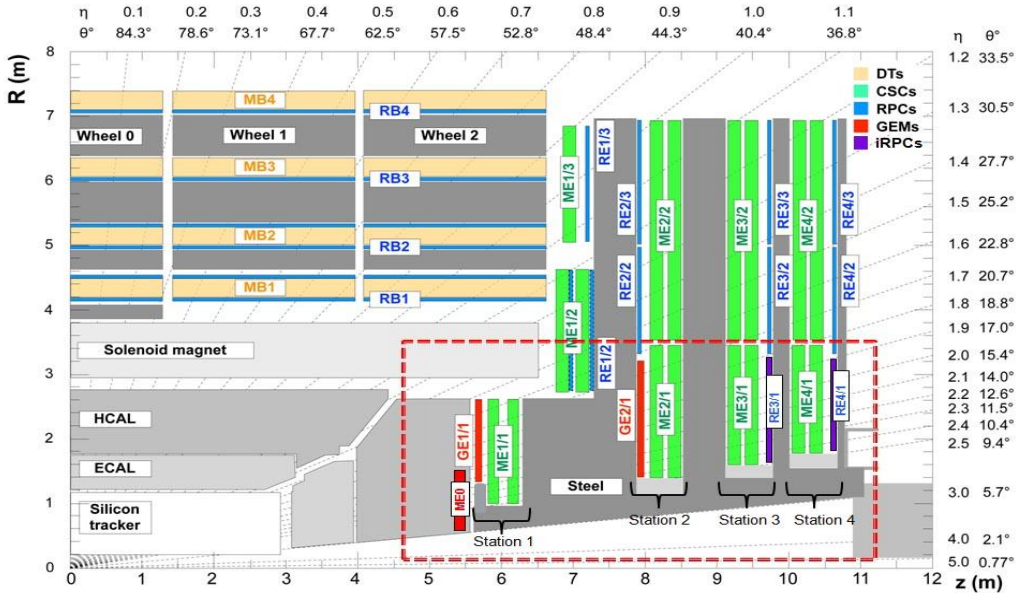

Figure 1: R-z cross section of a quadrant of the CMS detector

1.1 LONGEVITY STUDY FOR THE PRESENT RPC SYSTEM

The present RPC system has been certified for 10 LHC years operation [6], a new irradiation campaign is needed to confirm that it will survive to the harsher background conditions expected at HL-LHC. Based on Run2 data and assuming a liner dependence of the background rates as a function of the instantaneous luminosity, the expected rates and integrated charge at HL-LHC are about 600 Hz/cm^2 and 840 mC/cm^2, respectively (including a safety factor of three).

In July 2016, four spare Endcap chambers (two RE2/2 and two RE4/2 chambers) have been installed at the new Gamma Irradiation Facility (GIF++) at CERN. This facility is equipped with a Cs-137 gamma source of 14 TBq (in 2015) activity and a system of movable filters that allows to variate the gamma irradiation conditions, providing a fairly realistic simulation of the HL-LHC conditions. A 100 GeV muon beam, providing excellent probes for detector performance studies, complements the source. Two chambers, out of the fours (one RE2/2 and one RE4/2), are continuously operated under gamma irradiation, while the remaining two chambers are turned on only from time to time and used as reference. The integrated charged as a function of the time is showed in Figure 2. At present one chamber integrated one equivalent of HL-LHC charge (without safety factor) and we plan to reach the 3 times the HL-LHC charge by end of 2018.

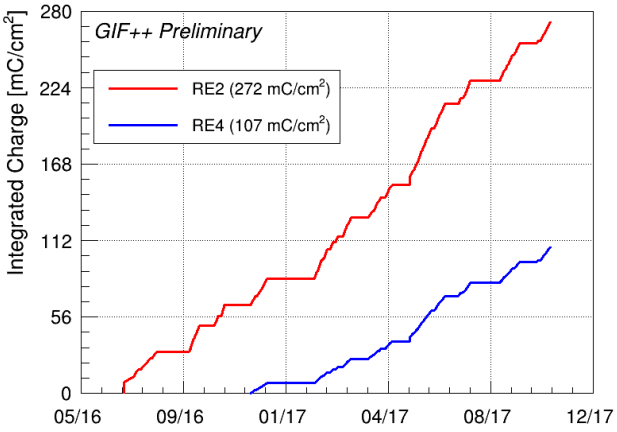

Figure 2: RE2/2 (red) and RE4/2 (blue) integrated charge versus time

Since the beginning of the irradiation test, I am in charge to monitor the detector parameters (counting rates and currents in several background conditions, noise and dark current, electrode resistivity) on the irradiated and not irradiated detectors.
The rates and the currents are, periodically, measured. To cancel out the dependence on the environmental conditions, the ratio of irradiated and reference chambers is measured as a function of the integrated charge and reported in Figure 3 (left) for the current and in Figure 3 (right) for the rate. The measurements show that there is no impact of the irradiation on the performance of the detector for both RE2/2 and RE4/2 chambers. The difference in the ratio between the two chambers is due to the different relative position of RE2/2 (red circles in the figure) and RE4/2 (blue squares) chambers with respect to the reference chambers inside the GIF++ zone.

In order to spot variations of electrode surface due to the irradiation, the detector noise rate and dark current is also measured. The current and rate versus the integrated charge for the RE2/2 irradiated chamber are showed in Figure 4. No significant variations have been observed so far.

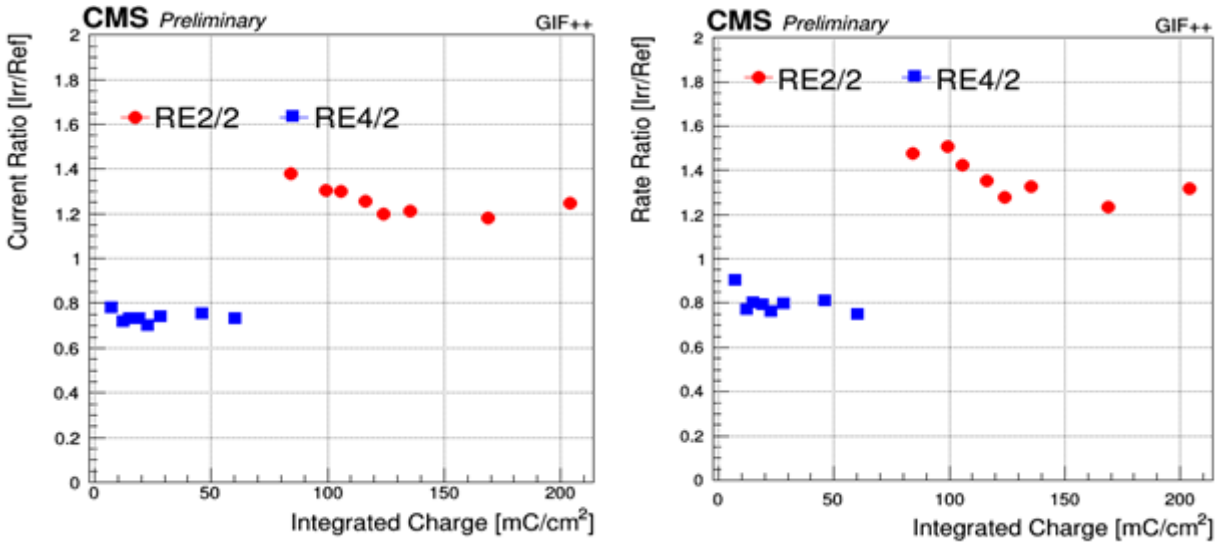

Figure 3: Current ratio between irradiated and non-irradiated reference chambers as a function of the integrated charge (left). Rate ratio between irradiated and reference chambers as a function of the integrated charge (right). Red circles correspond to RE2/2 chambers, blue squares to RE4/2. The difference in the ratio between RE2/2 and RE4/2 chambers is due to the different relative position of the chambers with respect to the reference chambers.

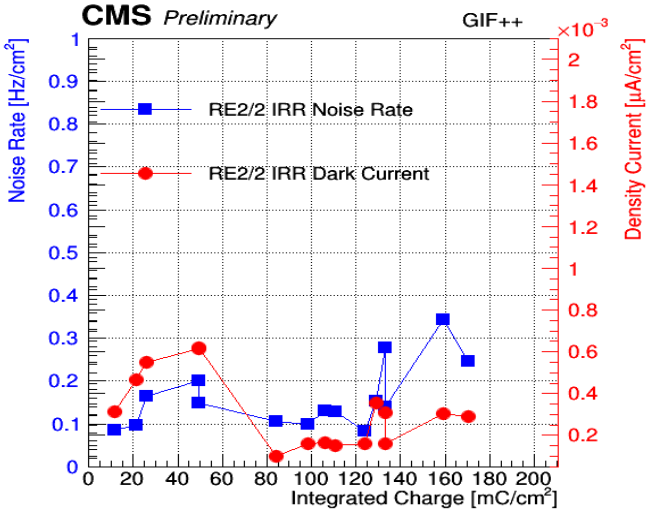

Figure 4: Noise rate (blue squares) and dark current (red circles) versus integrated charge collected during the GIF++ studies for the RE2/2 irradiated chamber.

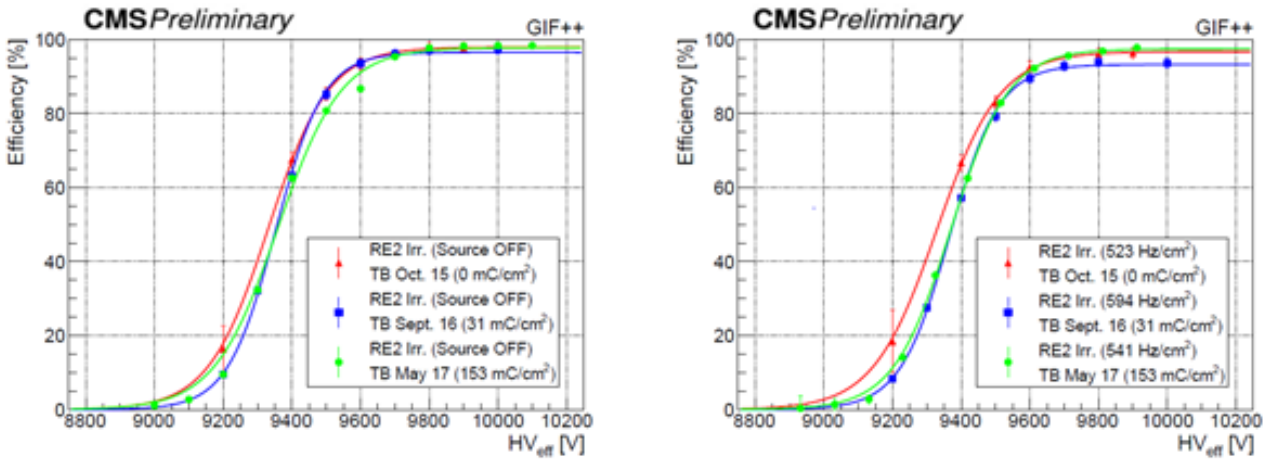

Figure 5: RE2/2 hit efficiency as a function of the effective High Voltage taken with no irradiation (left) and under a gamma background rate of about 600 Hz/cm2 (right). The efficiency of the RE2/2 chamber is measured corresponding to different periods of irradiation (0, 31 and 153 mC/cm2).

When muon beam is available, the performance of the irradiated and reference detectors are being studied. In Figure 5, the hit efficiency of the RE2/2 chamber as a function of the effective HV taken with no irradiation (left) and under gamma background rate of about 600 Hz/cm2 (right), is reported after different periods of irradiation at GIF++. The working point, defined as the voltage value at which 95% of the maximum efficiency is reached, is unchanged after different periods of irradiation, both under 600 Hz/cm2 and without gamma background rate. Figure 6 shows the hit efficiency (left) and the cluster size defined as the number of fired strip per hit (right) for the RE2/2 chambers (for the two irradiated and for the two non-irradiated reference chambers) at the working point as a function of the background rate. For all detectors the efficiency is stable in time with a small decrease (2%) of the efficiency at the highest expected background rate of 600 Hz/cm2. The measurements have been repeated after different periods of irradiation corresponding to 4.5% (31 mC/cm^2) and 18% (153 mC/cm^2) of the total integrated charge expected by the end of HL-LHC.

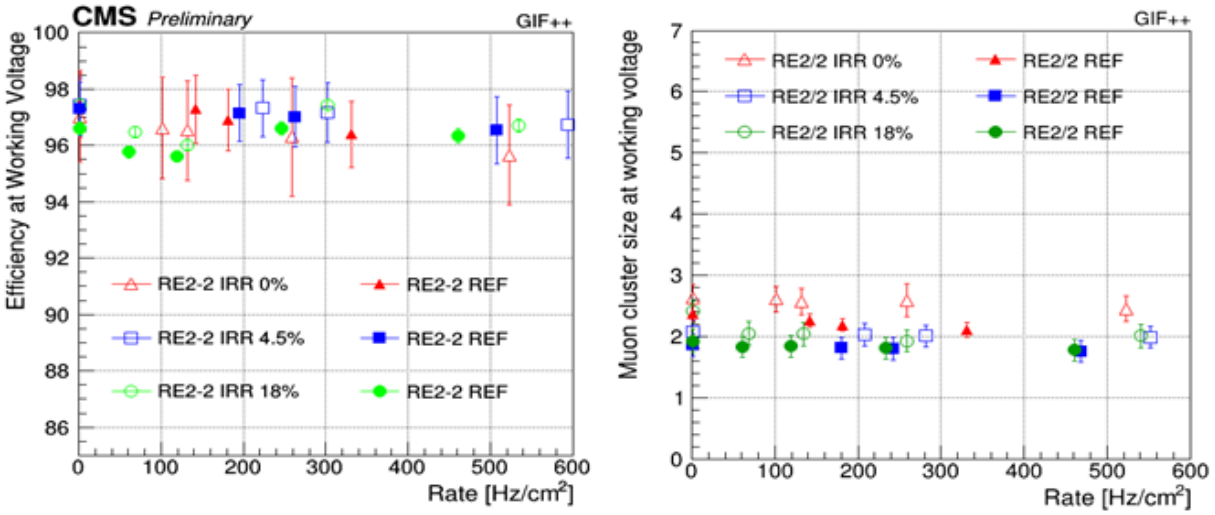

Figure 6: Evolution of the hit efficiency (left) and cluster size (right) at the HV Working Point, for RE2/2 chambers as a function of the γ rate per unit area. Both irradiated and non-irradiated reference chambers are shown. The measurements have been repeated after different periods of irradiation (corresponding to 4.5% and 18% of the total integrated charge expected by the end of HL-LHC).

1.2 RPC SYSTEM EXTENSION AT THE HIGH ETA REGION 1.8 < | η | < 2.4

The RPC system will extend the muon eta acceptance from | η | = 1.9 to 2.4 in order to complement the existing ME3-4/1 stations, equipped with CSC only, increasing the muon system redundancy, and to extend the contribution of RPCs for both muon tracking and triggering in the forward region. The two stations RE3/1 and RE4/1 will be equipped with a new generation of improved Resistive Plate Chamber (iRPC), which must be able to sustain the background conditions, around 2 kHz/cm^2, expected at HL-LHC. From the design point of view, the chambers are similar to the existing wedge-shaped Endcap RPC detectors, each spanning 20° in φ with radially oriented readout strips. Thus, the iRPC project adds 18 new chambers per muon disk, or 72 chambers in total for the RE3/1 and RE4/1 stations in both Endcap.

During last years, several RPC prototypes have been built using similar technology of the present RPC but having different geometry configurations (thinner gas gap and electrodes thickness) and electrode materials. Shortening the recovery time of the electrodes and reducing the total charge produced in a discharge will achieve the higher rate capability with respect to the current RPC detectors. Extensive tests performed at GIF++ allowed to define the baseline for the iRPC: double gas gap with HPL electrodes as the present RPC but having a lower resistivity in the range from 0.9 to 3 10^{10} Ω·cm (from 1 to 6 10^{10} Ω·cm); the electrodes and gas gap both reduced, from a thickness of 2 mm in the current design, to 1.4 mm. The lower charge produced per traversing particle will also reduce the integrated charge deposited and slow down aging. Furthermore, the operational high voltage is lowered improving the robustness of the system. In May 2017, a large size trapezoidal chamber has been tested at GIF++ with a muon beam to validate the performance under different background conditions. In Figure 7 the efficiency and the average cluster size are plotted as a function of the applied effective voltage, in absence of background (left plot) and with a gamma background rate of 2 kHz/ cm^2 (right plot). The shift in the working voltage is confirmed to be less than 300 V while the efficiency remains slightly above 95% also under the maximum background rate.

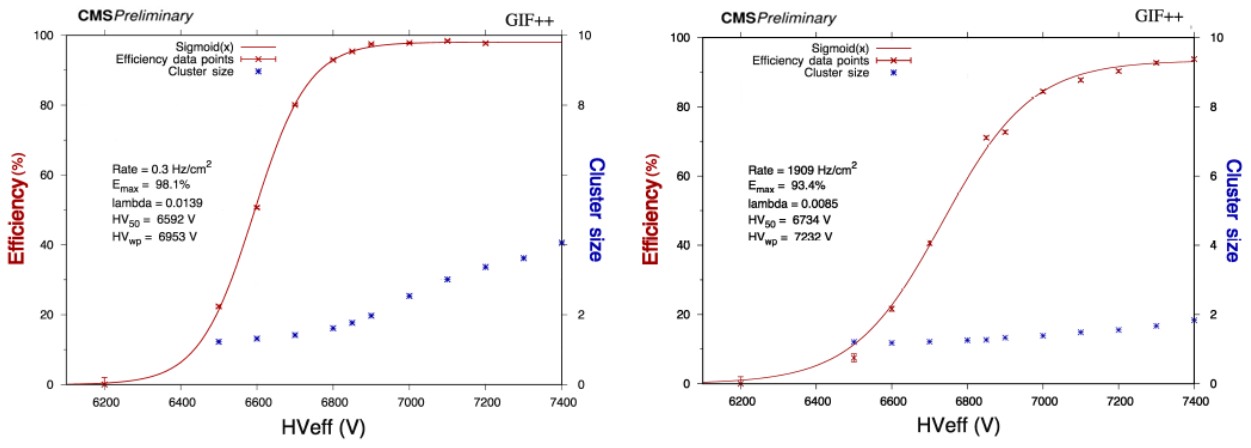

Figure 7: Efficiency and average cluster size of a 1.4 mm double-gap RPC large size chamber as a function of the effective voltage, tested without gamma background (top) and under a gamma background rate of 2 kHz/cm^2 (bottom). The data were measured at the fixed threshold of 300 mV and fitted with a sigmoidal function.

In this context, in order to have a better estimation of the expected background condition at HL-LHC in the new stations 3/1 and 4/1, I am studying the sensitivity of the iRPC at CMS background conditions considering the different particles (gammas, neutrons and electrons) and energy spectrum. The detector sensitivity is defined as the probability for a background particle ($N_{background}$) at a given energy, reaching the surface of the iRPC, to producing a signal in the detector (N_{RPC}):

$$S(E) = \frac{N_{RPC}}{N_{background}} \qquad [1]$$

As first step, I started to study the sensitivity of the iRPC at the GIF++ gamma energy both by Monte Carlo simulated method and experimentally. For this purpose I described the iRPC geometry and all detectors present in the GIF++ area during the May 2017 test beam, with the GIF++ GEANT4 simulation package [7,8]. Figures 8 shows the picture and the simulation of the GIF++ area, the iRPC under test and the others set-up.
The gamma irradiator source model is shown in detail in Figure 9 (left), including all components, such as the source capsule, collimator, lens and filters system. The filters system consist of three planes of filters, with three filters per plane are installed (Figure 9 right). The planes have a convex shape and they are movable. The different filters positions configurations allow reducing the gamma flux with different absorption factor (ABS), from a factor 1 to a factor 46000. The ± 37° panoramic collimators and the angular correction lens allow to replace the $1/r^2$ dependence of the photons current by a uniform current in each X-Y plane orthogonal with respect the source. The uniform gammas incident distribution on the detector surface is confirmed by the simulation, as shown in Figure 10 left, and by the electrons creation and ionization in the detector gaps shown in Figure 10 right.

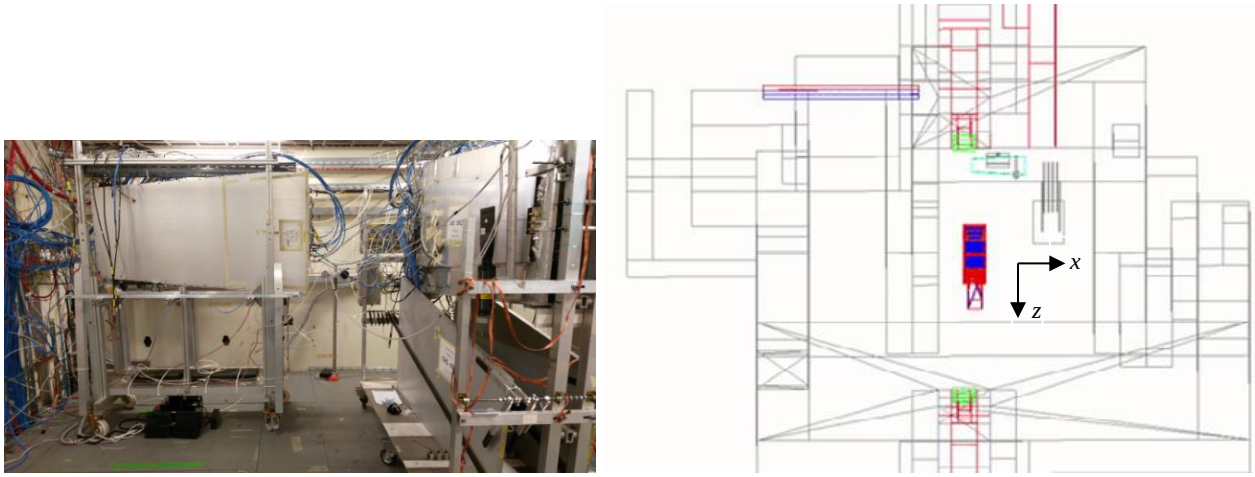

Figure 8: Picture of GIF++ area with inside the iRPC and others set-up(left) and simulated geometry, including the detectors, implemented in the Monte Carlo simulation (right).

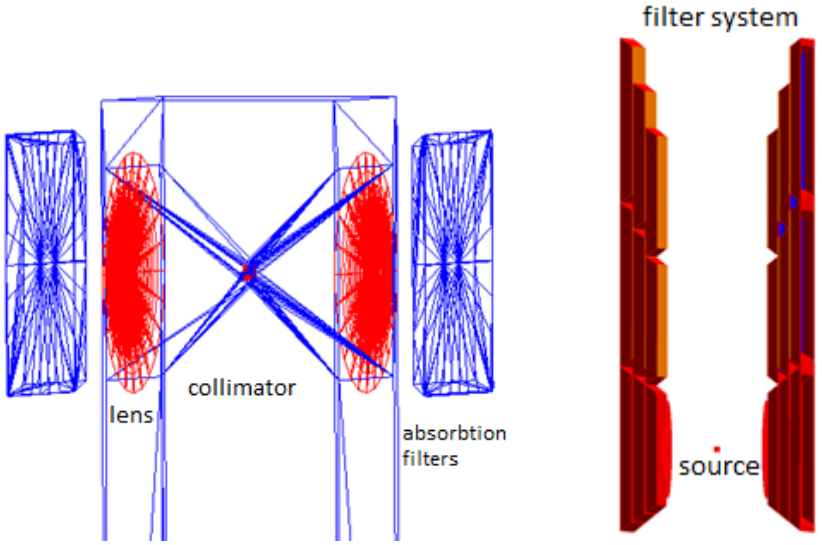

Figure 9: Model of the GIF++gamma irradiator used in the simulation, composed by the source capsule, collimator, lens and absorption filters (left), and detailed schema of the filter system (right)

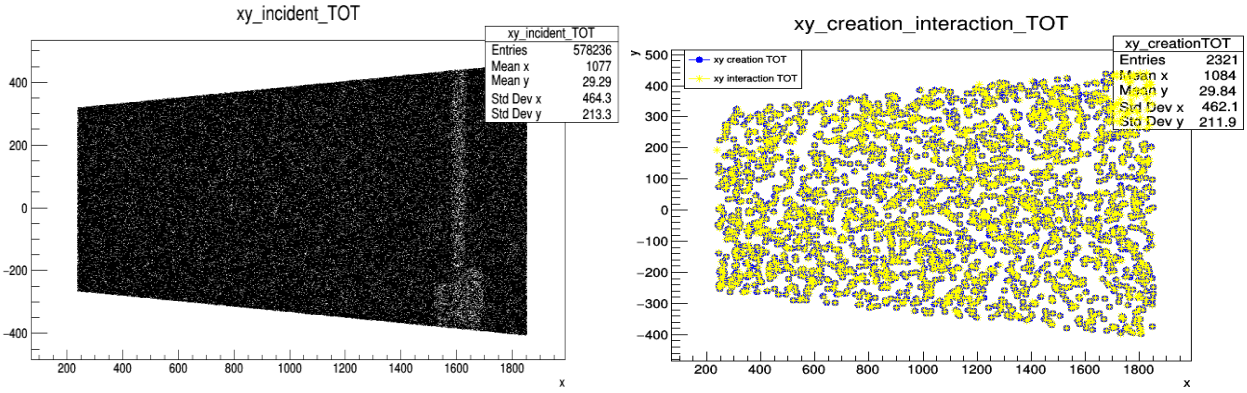

Figure 10: XY spatial distribution of the incident gammas on the detector surface (left), and XY spatial distribution of the creation and ionization of the electrons that produce a signal in the detector (right).

The simulation allows us to obtain many interesting information, such as the number of the incident particles on the detectors surface, the XY spatial distribution of the incident particles, the particles direction, the kinetic energy of the incident particles, the kinds of particle, if it is a primary or secondary particle, the process that created the incident particles, the number of electrons created in each gaps, the spatial distribution of the electrons in the gaps when they are created and when they ionize, the kind of the process for the electrons creation and ionization, the kinetic energy of the electrons, etc.

In figure 11, the GIF++ photon energy distribution is shown. The distributions are obtained performing a simulated run applying a low absorption factor (high rate), ABS 4.6 in red, and a high absorption factor (low rate), ABS 1000 in blue. The number of events has been normalized. The nominal kinetic energy of the photons produced by the Cs-137 decay from the source is 662 keV, but the photon current is modified by the interaction of photons with the materials present in the

GIF++ facility, mainly lead (irradiator, filters), steel (filters, floor), aluminium (filters) and concrete (sur- rounding bunker enclosure). For the available photon energies of 662 keV or below, the main processes involved are Compton scattering and photoelectric effect. Through collisions with electrons of dense materials, photons may lose a fraction of their energy along their travel. Therefore, in addition to the monochromatic 662 keV photons from Cs-137, a low energy component of degraded photons develops within the irradiator. This low energy component is already present when the photons emerge from the small thin-walled capsule containing the active material. Interactions in the material subsequently traversed further modify the spectral shape of degraded photons. A part the pick at the nominal energy value is possible to distinguish two others picks: at 80 keV and at 184 keV. Following the gammas photoelectric effect in lead, which compose many part of the filter system and the collimator, there is a high probability for the gammas having energy in the range 0-300 keV that the lead atom de-excites by emitting fluorescent X-rays from K-shell having an energy around 80 keV. Concerning the second pick, all photons emitted by the irradiator will interact with the surrounding material in the bunker and will finally be absorbed. The photons that are not absorbed when impinging on a wall, but manage to re-enter into the bunker, are called albedo photons. They are expected to be mainly back-scattered photons from Compton scattering. For the photons that collide with a nearly free electron, the lowest energy of the scattered photon corresponds to a scattering angle of 180°. For 662 keV photons this leads, independent of the wall material, to a back-scattered photon of about 184 keV, which correspond to the second, pick. Photons back scattered at other angles will have somewhat higher energy. Inside the wall, before emerging again, the photon may suffer further Compton scatterings, which will lower the energy of the albedo photon. Also incident photons of energies lower than 662 keV will extend the albedo spectrum to lower energies. In conclusion, a high absorption factor attenuates the photon current but the energy photons degradation will be larger and the number of photons having the nominal energy values less.

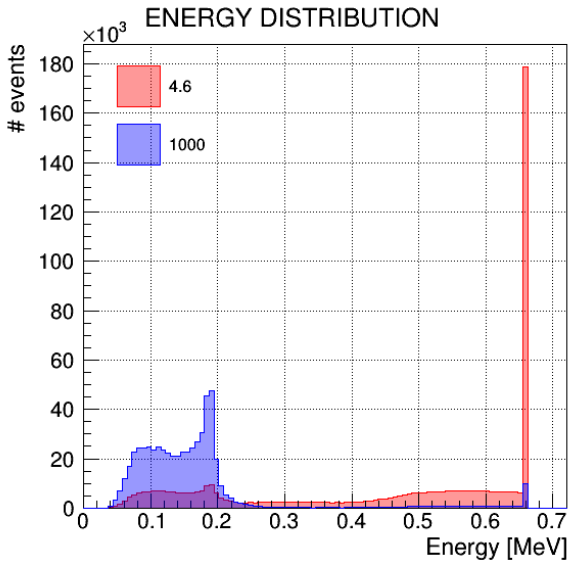

Figure 11: GIF++ gamma energy spectrum applying an high absorption factor 1000 (blue) and a low absorption factor 4.6 (red).

The position where the primary electrons are produced and where they ionize interacting in the gas gaps was studied. In the Figure 12, the position along the detector thickness (Z direction), for both gas gaps, where the electrons are produced after the interaction of the incident gammas with the detector materials (blue gap1 and red gap2), and where the electrons ionize in the gas gap (yellow gap1 and green gap2) is plotted. Most of the electrons, which produce a signal in the gas-gap, are produced in the last 200-300 μm of 1.4 mm electrode. For this reason we do not expect a significant difference in the sensitivity of the iRPC with respect the standard CMS-RPC which have 2 mm of electrodes thickness.

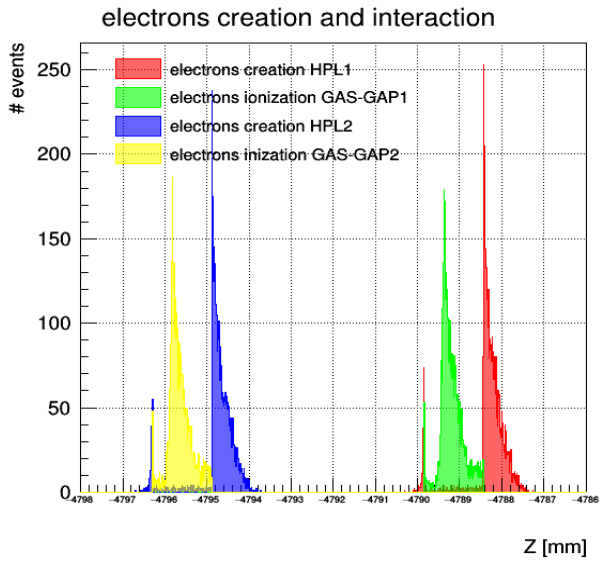

Figure 12: Z position for the electrons creation an ionization (left), and energy deposited as a function of the detector thickness (Z direction).

In order to validate the simulation, the detector counting rate has been experimentally measured at different absorption factors, defined as the number of fired strips divided for the cluster size. Because in the simulation we assume 100% the detector efficiency at ionizing particles, the counting rate has been corrected adding a fraction of rate lost due to the detector inefficiency:

$$R_{corrected} = \frac{Hit\ Rate}{Cluster\ size} + Rate_{inefficiency} \qquad [2]$$

From simulation point of view the events that produce a signal in the detector is given when an electron ionizes in one of the two gas gaps or both.

In Figure 13 left, the comparison between data (in red) and simulation (in blue and green) rate is shown as a function of the ABS. For the simulated data two cuts on incident photons energy cut of 500 keV and 600 keV have been applied. In Figure 13 right the sensitivity simulated and measured, as defined in [1], are reported as a function of the ABS. The good agreement between experimental and simulated data, in the worst case the discrepancy is a factor 1.5, validated the simulation.

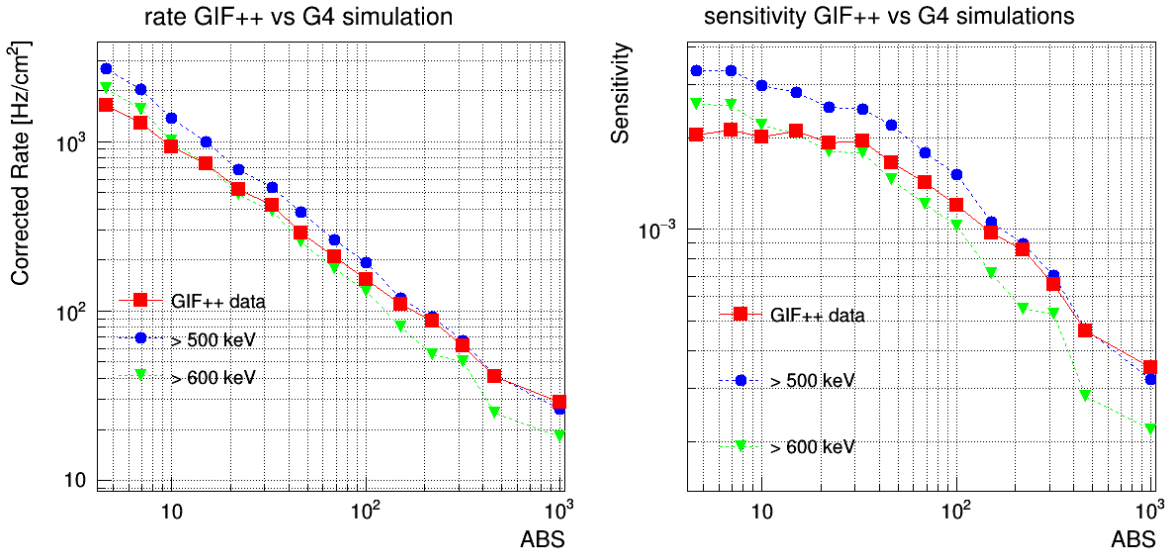

Figure 13: Rate (left) and sensitivity (right) comparison between experimental data from GIF++(read squares) and simulated data applying a cut energy of >500 keV (bue circles) and >600 keV (green triangles).

REFERENCES

[1] CMS Collaboration, *The Compact Muon Solenoid Technical Proposal*, CERN/LHC 94-38, 15 December 1994.

[2] CMS Collaboration. *The CMS experiment at CERN LHC*, JINST 3 (2008).

[3] CMS Collaboration, *The Muon Project, Technical Design Report*, CERN/LHCC 97-32, CMS TDR 3 (1997).

[4] CMS Collaboration, *Phase-2 Technical Proposal*, CERN-LHCC-2015-010, LHCC-P-008.

[5] CMS Collaboration, *Upgrade of CMS detector through 2020 Technical Proposal*, CERN/LHC 2011-06, CMS UG-TP-1 (2011).

[6] *The Large Hardon Collider Accelerator Project*, LHC CERN-AC-93-03.

[7] D. Pfeiffer, *The radiation field in the Gamma Irradiation Facility GIF++ at CERN*, *arXiv:1611.00299v3*, 8 June 2017.

[8] GEANT4, *http://geant4.cern.ch/*

2. *FUTURE PLAN*

- **Monte Carlo simulation:**
  The simulation will be completed by estimating the iRPC sensitivity with respect to gammas, neutrons and charged particles, for the energy spectrum and angular distribution in the CMS high eta region as expected at HL-LHC. The sensitivity will be then used to scale the background fluxes expected in CMS at HL-LHC.
- **Present RPC system longevity study:**
  The already started longevity study on spare RPCs will continue in order to validate the system for the phase II. Plan to reach the expected integrated charge at HL-LHC in one year.
- **iRPC longevity study:**
  A dedicated longevity campaign will start in order to study the longevity of the iRPC as a function of the integrated charge expected at HL-LHC and to validate this detector technology for the entire period running.
- **Ecogas:**
  In order to reduce the gas emissions, mainly coming from the $C_2H_2F_4$ (95% of the RPC gas mixture), a gas with high Global Warming Potential (GWP), a new test with ecological gas mixtures with lower GWP, will start next year. Plan is to validate performance and aging of the new gas mixture at GIF++.

3. *CONFERENCES*

Following the list of my presentations at conferences during the first PhD year:

1. ***"Upgrade of the RPC system of the CMS Muon Spectrometer",*** ”SIF2017: Congresso nazionale società italiana di fisica”**, Trento, Italy, September 2017**

2. ***"Upgrade of the RPC system of the CMS Muon Spectrometer",*** **”2017 Fall Meeting of the Korean Physical Society”, Gyeongju-si, Korea, October 2017**

4. *SCHOOLS, WORKSHOPS AND SEMINARIES*

During the first PhD year I participated to the following workshops, seminaries and schools:

4.1 ***SCHOOLS***

1. ***“XIV Seminar on Software for Nuclear, Subnuclear and Applied Physics”***, Alghero, Italy, June 2017
2. ***“CMS Physics Object School POS”***, Bari, Italy, September 2017, participating as facilitator and giving a lesson about the introduction of “GEANT4” and a short exercise

4.2 WORKSHOPS

1. ***"RPC workshop”***, CERN Geneva, Switzerland, November 2016
2. ***"RPC Upgrade workshop”***, CERN Geneva, Switzerland, March 2017

3. ***"Muon phase II Upgrade workshop"***, CERN Geneva, Switzerland, March 2017
4. ***"2nd RPC Upgrade workshop"***, CERN Geneva, Switzerland, May 2017
5. ***"Muon Upgrade workshop"***, CERN Geneva, Switzerland, June 2017

4.3 SEMINARIES

1. ***"Last results about BSM in the Higgs scalar sector and beyond"***, Bari, Italy, May 2017
2. ***"The big picture of the particle physics"***, Bari, Italy, September 2017

5. PhD COURSES

During the first Phd year, I followed the eight courses corresponding to a total of 16 CFU. Title and status of the exams are reported in the Table 1:

Course	CFU	Status
LHC Phenomenology	2	Passed
Gas detectors	2	Passed
Programming with Python	2	Passed
How to prepare a technical speech in English	2	Passed
European research model and promotion of research results	2	Passed
Labview introductory course	2	Passed
Interpolation methods and techniques for experimental data analysis	2	Passed
C++	2	Passed

Table 1: Courses